Computationally efficient dielectric calculations of molecular crystals

Kathleen A. Schwarz,[1, a)] Ravishankar Sundararaman,[2] and T A Arias[2]
[1)] *Department of Chemistry and Chemical Biology, Cornell University, Ithaca, NY 14853*
[2)] *Department of Physics, Cornell University, Ithaca, NY 14853*

(Dated: 19 May 2015)

The microscopic dielectric response is a key quantity for electronic materials such as organic semiconductors. Calculations of this response for molecular crystals are currently either expensive, or rely on extreme simplifications such as multipole expansions which lack microscopic detail. We present an alternate approach using a microscopic analogue of the Clausius-Mossotti equation, which constructs the dielectric response of a crystal from an eigenvalue decomposition of the dielectric response of individual molecules. This method can potentially be used to examine the effects of defects, disorder and surfaces on the dielectric properties of molecular solids.

I. INTRODUCTION

Recent advances in organic electronics have spurred interest in molecular solids and liquids for dielectric and optical applications.[1–3] The behaviors of these materials are typically assessed through experiments, although the performance of these materials can be altered by uncharacterized structural defects and impurities.[4] A computational approach to better understand and predict the dielectric and optical properties of these materials would complement experimental work, facilitating further advances in the characterization and design of new materials.

Current state-of-the-art solid state dielectric calculations are limited to systems smaller than a typical molecular crystal of interest in organic electronics, or the calculations rely on simplifications that discard microscopic information (see for instance Ref. 5). Quantum chemistry calculations also have molecule size limitations, and additionally have basis-set convergence issues, particularly for the dielectric response. They also do not have a systematic way to deal with the environment surrounding the molecule. Additionally, current computational approaches do not leverage the repeated molecular structure of molecular crystals and liquids, requiring independent calculations for molecules in crystal polymorphs, and in different molecular configurations of a liquid.

The repeated structure of molecular crystals presents an opportunity that has not yet been exploited, except for in limited contexts. For instance, a tight-binding approach that uses atomic dielectric eigenfunctions as a basis has been shown to work well for an isolated beryllium dimer.[6] Here, we describe a method to calculate the optical dielectric response of molecular crystals and liquids that takes full advantage of the modularity of these systems. In essence, we show that the microscopic dielectric response of a molecular crystal can be assembled from the microscopic dielectric response of its constituent molecules. This method enables response calculations of large molecular crystals and liquid configurations, with far less computational cost than equivalently-converged direct calculations.

We limit our application to the microscopic electronic response at fixed ionic positions, which is a key quantity of interest in the calculation of electronic correlation energy within the random phase approximation (RPA).[6–8] We compare dielectric band structures,[9] the inverse dielectric function eigenvalues as functions of the wave vector, computed within our approach against direct calculations for crystals to evaluate the accuracy of our approach. Further, as is standard in studies of dielectric band structure approximations,[9,10] we focus on the static electronic response for simplicity and definiteness; incorporating frequency dependence in the electronic response is straightforward.

We begin with a general introduction to the theory of microscopic dielectric response in section II, and present the key idea of separating that response into molecular contributions in section II A. Section II B presents the theoretical framework for combining molecular responses into that of the crystal, and section II C describes how to extract the macroscopic dielectric response from the microscopic one. Finally, section III applies this method to calculate the macroscopic as well as microscopic dielectric response of the extremely-polar ice and the non-polar benzene crystals, and demonstrates its accuracy in comparison with direct response calculations for these widely different solids.

II. THEORY

The full inverse microscopic dielectric matrix $\epsilon^{-1}(r, r')$, the central quantity in describing the dielectric response of a system, expresses the linear response ϕ_{tot} of the total electrostatic potential to the application of an external potential ϕ_{ext} through

$$\phi_{\text{tot}}(r) = \int d^3r'\, \epsilon^{-1}(r, r')\phi_{\text{ext}}(r'). \tag{1}$$

In the following discussion, we find it convenient to employ a representation-independent, operator-based nota-

[a)] Electronic mail: kas4@nist.gov

tion, so that (1) appears as $\phi_{\rm tot} = \epsilon^{-1}\phi_{\rm ext}$.

The operator most directly accessible to microscopic calculations is the external susceptibility $\chi_{\rm ext}$, which gives the first-order induced change in the charge density $\rho_{\rm ind}$ through the linear-response relation $\rho_{\rm ind} = \chi_{\rm ext}\,\phi_{\rm ext}$. Given this response function, one can then compute the corresponding induced potential, $\phi_{\rm ind} = K\rho_{\rm ind}$, where the Coulomb operator $K(r,r') \equiv 1/|r-r'|$ in the standard atomic units in which we work. It is also useful to define a total susceptibility $\chi_{\rm tot}$ that describes the linear response of the charge density to the total response potential, $\rho_{\rm ind} = \chi_{\rm tot}\phi_{\rm tot}$.

Substitution of the above relations into the decomposition of the total response potential, $\phi_{\rm tot} = \phi_{\rm ind} + \phi_{\rm ext}$, yields the standard connections between the microscopic dielectric response and susceptibility functions,

$$\epsilon^{-1} = 1 + K\chi_{\rm ext} \tag{2}$$

$$\epsilon = 1 - K\chi_{\rm tot}. \tag{3}$$

This also implies a Dyson relation for $\chi_{\rm ext}$ in terms of $\chi_{\rm tot}$,

$$\chi_{\rm ext} = \chi_{\rm tot} + \chi_{\rm ext}K\chi_{\rm tot}. \tag{4}$$

At this stage, no approximations have been made. In principle, $\chi_{\rm ext}$ can be extracted directly from correlated electronic structure methods, such as coupled-cluster (CC) or quantum Monte Carlo (QMC), by observing the response of the system under consideration to the application of a (large) set of perturbing potentials. However, this approach becomes prohibitive for all but the smallest systems.

Electronic band-structure approaches, while much more practical, unfortunately do not give direct access to $\chi_{\rm ext}$ or $\chi_{\rm tot}$. They instead provide $\chi_{\rm ni}$, the response of an effective non-interacting system of orbitals to changes in their external potential, which has the explicit form

$$\chi_{\rm ni}(r,r') = \sum_{i\neq j}(f_i - f_j)\frac{\psi_i^*(r)\psi_j(r)\psi_j^*(r')\psi_i(r')}{\epsilon_j - \epsilon_i}, \tag{5}$$

where $f_i \in [0,1]$ is the occupation and ϵ_i is the eigenvalue of the $i^{\rm th}$ band. The Kohn-Sham theorem[11] ensures that the density-response of such a non-interacting system to changes in the self-consistent Kohn-Sham potential, $\delta V_{\rm KS}$, gives the exact density response of the fully interacting system, so that $\rho_{\rm ind} = \chi_{\rm ni}\delta V_{\rm KS}$ exactly.

The first-order response of the Kohn-Sham potential includes responses in the external, Hartree, and exchange-correlation components

$$\delta V_{\rm KS} = \phi_{\rm ext} + K\rho_{\rm ind} + K_{\rm xc}\rho_{\rm ind} \tag{6}$$

$$= \phi_{\rm tot} + K_{\rm xc}\rho_{\rm ind}, \tag{7}$$

where $K_{\rm xc}(r,r') \equiv \delta^2 E_{\rm xc}/(\delta\rho(r)\,\delta\rho(r'))$ gives the response of the exchange-correlation potential to changes in the electron density. Combining these forms for $\delta V_{\rm KS}$ with $\rho_{\rm ind} = \chi_{\rm ext}\phi_{\rm ext}$ and $\rho_{\rm ind} = \chi_{\rm tot}\phi_{\rm tot}$, yields the following exact Dyson relations for the microscopic susceptibilities,

$$\chi_{\rm ext} = \chi_{\rm ni} + \chi_{\rm ni}(K + K_{\rm xc})\chi_{\rm ext} \tag{8}$$

$$\chi_{\rm tot} = \chi_{\rm ni} + \chi_{\rm ni}K_{\rm xc}\chi_{\rm tot}. \tag{9}$$

These can then be combined with (2,3) to yield the microscopic dielectric response.

Even with the relative economy of band-structure based methods, the standard approach of going from (5) through (8,9) and finally to (2,3) is limited to relatively simple systems due to the need to compute a prohibitive number of empty bands to converge the sum in (5). While a number of interesting approaches for decreasing these costs have been proposed,[12–14] these approaches would still require separate electronic band-structure calculations for each configuration of a liquid, or for each defect studied in a molecular crystal. A more efficient method for the dielectric response of solvated or molecular crystalline systems would thereby open a new range of problems for first principle studies.

A. Molecular separation ansatz

The first key observation of this work is that both $\chi_{\rm ni}$ and $\chi_{\rm tot}$ can be well-approximated as sums of independent localized molecular contributions for closed-shell molecular systems. This results in a radical simplification of the calculations necessary to determine the dielectric properties of a molecular crystal or liquid. This decomposition also provides, for the first time, a practicable method for including high-order electron-correlation effects into the dielectric response of large collections of molecules.

The efficacy of the decomposition of $\chi_{\rm ni}$ into a sum

$$\chi_{\rm ni}(r,r') = \sum_R \chi_{\rm ni}^{[m]}(r-R, r'-R) \tag{10}$$

of individual molecular density-response functions $\chi^{[m]}(r,r')$ stems directly from the structure of (5) for closed-shell molecular systems. For such systems, the relative electronic isolation of the molecules ensures little dispersion in the eigenvalues ϵ_i, allowing for unitary transformation among the bands to maximally localized orbitals, without affecting the value of either the i or j sums in (5). Moreover, under these conditions, the maximally localized orbitals will closely resemble the molecular orbitals so that, to a good approximation, the i and j sums can be taken to range over the molecular orbitals of the system. Finally, the relative lack of overlap between orbitals on different molecules ensures that both factors $\psi_i^*(r)\psi_j(r)$ and $\psi_j^*(r')\psi_i(r')$ in the numerator of (5) will be small. Therefore, only terms with i and j on the same molecule contribute significantly to the final result. Keeping only these terms and replacing the orbitals and eigenvalues with the corresponding molecular quantities then leads directly to (10).

The observation that $\chi_{\rm tot}$ may likewise be decomposed,

$$\chi_{\rm tot}(r,r') = \sum_R \chi_{\rm tot}^{[m]}(r-R, r'-R) \tag{11}$$

follows from Dyson iteration of (9). Because the major contributions to $E_{\rm xc}$ are reasonably well-approximated by local- or semilocal- density functionals, we expect that $K_{\rm xc}(r,r')$ only weakly connects points r and r' residing on different molecules. This, combined with the above anticipated decomposition of $\chi_{\rm ni}^{[m]}$ into localized molecular contributions, ensures that iteration of (9) does not generate strong inter-molecular connections in $\chi_{\rm tot}$. Therefore, a molecular decomposition of $\chi_{\rm tot}$ analogous to (10) should also yield a good approximation. Ultimately, the suitability of such molecular decompositions of $\chi_{\rm ni}$ and $\chi_{\rm tot}$ can only be evaluated through calculations of realistic systems, as we perform below.

The second key observation in this work is that the collection of the eigenfunctions of the non-interacting response function $\chi_{\rm ni}^{[m]}$ from each individual molecule m in the system provides a well-converging, albeit non-orthogonal, basis for dielectric response calculations. Although similar susceptibility eigenbasis approaches have been pursued in the past,[15–17] this work is the first to exploit the significant computational advantages of the decomposition into individual molecule response functions. Here, we represent the eigen-decomposition of the non-interacting molecular susceptibility of each molecule m as

$$\chi_{\rm ni}^{[m]} = V^{[m]} X_{\rm ni}^{[m]} V^{[m]\dagger}, \tag{12}$$

where $X_{\rm ni}^{[m]}$ is a diagonal matrix containing the eigenvalues and $V^{[m]}$ is a matrix containing the eigenfunctions, arranged so that the $n^{\rm th}$ column of $V^{[m]}$ contains a convenient numerical representation of the $n^{\rm th}$ eigenfunction, such as real-space samples or a plane-wave expansion. Finally, in this expression, the $\dagger$ operator implements the integral overlap between eigenfunctions so that $V^{[m]\dagger}V^{[m]} = I$, the identity.

Dyson iteration of (8,9) then establishes that both the external and total molecular susceptibilities take the form (12), with matrix elements $X_{\rm ext}^{[m]}$ and $X_{\rm tot}^{[m]}$, respectively, obeying

$$X_{\rm ext}^{[m]} = X_{\rm ni}^{[m]} + X_{\rm ni}^{[m]}(\bar{K}^{[m]} + \bar{K}_{\rm xc}^{[m]})X_{\rm ext}^{[m]} \tag{13}$$

$$X_{\rm tot}^{[m]} = X_{\rm ni}^{[m]} + X_{\rm ni}^{[m]}(\bar{K}_{\rm xc}^{[m]})X_{\rm tot}^{[m]}. \tag{14}$$

Here, $\bar{K}^{[m]} \equiv V^{[m]\dagger}KV^{[m]}$ and $\bar{K}_{\rm xc}^{[m]} \equiv V^{[m]\dagger}K_{\rm xc}V^{[m]}$ are the matrix elements of the corresponding operators in the $V^{[m]}$ basis. Below we will demonstrate that the number of eigenvectors required is on the order of $10-20$ per valence electron and generally much smaller than the number of filled-empty pairs ij needed to converge the sum (5), so that the preceding relations are readily handled for realistic systems even on modest workstations.

To work within a density-functional theory framework, the matrix elements $X_{\rm ext}^{[m]}$ or $X_{\rm tot}^{[m]}$ are readily obtained by solving (13,14), yielding for example the easily computed expression $X_{\rm tot}^{[m]} = (1 - X_{\rm ni}^{[m]}\bar{K}_{\rm xc}^{[m]})^{-1}X_{\rm ni}^{[m]}$. In the case of a fully correlated method, one would compute $X_{\rm ext}^{[m]} = V^{[m]\dagger}(\chi_{\rm ext}V^{[m]})$ by first applying each column of $V^{[m]}$ as an external potential $\phi_{\rm ext}$ to the correlated molecular calculation. With $X_{\rm ext}^{[m]}$ in hand, one may then employ (4) to determine the total fully correlated molecular response function through $X_{\rm tot}^{[m]} = (1 + X_{\rm ext}^{[m]}\bar{K}^{[m]})^{-1}X_{\rm ext}^{[m]}$. In this way, several hundred correlated electronic structure calculations on a single molecule can be used to build up the fully correlated dielectric response function for large collections of molecules.

B. Crystal response

The treatment of periodic systems is best accomplished through transformation to a Bloch-periodic basis,

$$V(k) = \sum_m e^{ik\cdot R_m} V^{[m]}, \tag{15}$$

where k is the Bloch character of the particular basis formed, $V^{[m]}$ are the eigenfunctions for molecule m, R_m is the location of molecule m, and we take the R_m to form a periodic lattice.[18] One then obtains the standard result that, for functions of Bloch character k, the action of a full crystal operator of the additive forms (10,11) is equivalent to that of the operator

$$\chi(k) \equiv V(k)X^{[m]}V(k)^\dagger, \tag{16}$$

where the inner product associated with $\dagger$ now represents integration over the unit cell of the crystal lattice, rather than the entire space.

Analogously to the molecular results, Dyson iteration of (8,9) using the crystal form (16) leads to the conclusion that the operators $\chi_{\rm ext}(k)$ and $\chi_{\rm tot}(k)$ are also of the form (16), but with k-dependent matrix elements obeying

$$X_{\rm ext}(k) = X_{\rm ni}^{[m]} + X_{\rm ni}^{[m]}\left(\bar{K}(k) + \bar{K}_{\rm xc}(k)\right)X_{\rm ext}(k) \tag{17}$$

$$X_{\rm tot}(k) = X_{\rm ni}^{[m]} + X_{\rm ni}^{[m]}\bar{K}_{\rm xc}(k)X_{\rm tot}(k), \tag{18}$$

with $\bar{K}_{\rm xc}(k) \equiv V(k)^\dagger K_{xc}V(k)$ and $\bar{K}(k) \equiv V(k)^\dagger KV(k)$. And, analogously to (4), we find

$$X_{\rm ext}(k) = X_{\rm tot}(k) + X_{\rm ext}(k)\bar{K}(k)X_{\rm tot}(k). \tag{19}$$

When working with density-functional based methods, the matrices $X_{\rm ni}^{[m]}$ come directly from the molecular calculations and are thus k-independent and require no special calculation. The matrix elements $\bar{K}_{\rm xc}(k)$ are best computed directly in real space due to the (semi-)local nature of common exchange-correlation functionals. Finally, the matrix elements $\bar{K}(k) = V(k)^\dagger KV(k)$ are best computed in reciprocal space due to the extended nature of the Bloch basis functions.

For correlated methods, one simply substitutes the molecular matrix elements $X_{\rm tot}^{[m]}$, obtained as described

above, into the Bloch form for additive operators (16) yielding $\chi_{\rm tot}(k)$. Then, to obtain $\chi_{\rm ext}(k)$ one would employ the crystal Dyson equation (19), obtaining the matrix elements

$$X_{\rm ext}(k) = X_{\rm tot}(k)\left(1 - \bar{K}(k)X_{\rm tot}(k)\right)^{-1}. \tag{20}$$

Finally, armed with the matrix elements and Bloch representations (16) for $\chi_{\rm ext}(k)$ and $\chi_{\rm tot}(k)$, one may employ (2) and (3) respectively to build the full crystal dielectric response operators, yielding in the former case

$$\epsilon^{-1}(k) = 1 + KV(k)X_{\rm ext}(k)V(k)^\dagger. \tag{21}$$

The eigenvectors of $\epsilon^{-1}(k)$ must be linear combinations of the columns of $KV(k)$, and therefore we can compute the dielectric band structure directly as the eigenvalues of $1+[V(k)^\dagger KV(k)]X_{\rm ext} \equiv 1+\bar{K}(k)X_{\rm ext}(k)$, a matrix of manageable size that is explicitly computable from the results above.

C. Macroscopic equations

Determination of the macroscopic equations and dielectric tensor $\bar{\epsilon}$ requires connecting the scalar microscopic response theory to the macroscopic vector equations. This connection, in particular the $G \to 0$ limit, is rather complicated for general solids and is derived in detail in Ref. 10. Here, we derive a substantially simpler expression for molecular solids which is made possible by the localization of the induced polarization on constituent molecules.

In Fourier space, the Poisson equations for the macroscopic total potential $\bar{\phi}_{\rm tot}$ and macroscopic external potential $\bar{\phi}_{\rm ext}$ are $k^\dagger\bar{\epsilon}k\bar{\phi}_{\rm tot} = 4\pi\rho_{\rm ext}$ and $|k|^2\bar{\phi}_{\rm ext} = 4\pi\rho_{\rm ext}$, respectively, where k is the wave vector associated with the macroscopic perturbation. Equating the preceding relations yields $\hat{k}^\dagger\bar{\epsilon}\hat{k} = \bar{\phi}_{\rm ext}/\bar{\phi}_{\rm tot}$. Thus, the anomalous, directional dependence of the $k \to 0$ limit of the microscopic dielectric response reflects directly the tensor nature of the macroscopic dielectric constant.

The macroscopic fields in the above paragraph represent smooth functions, averaged over the unit cells of the crystal and thus exhibit only long-wavelength behavior. A suitable choice for the (applied) external potential is thus $\bar{\phi}_{\rm ext} = \phi_0 e^{ik\cdot r}$, or equivalently $\phi_{{\rm ext},G}(k) = \phi_0\delta_{G,0}$ where δ is the Kronecker delta function. The microscopic response of the material system to this applied potential, $\phi_{\rm tot} = \sum_G \phi_{{\rm tot},G}(k)e^{i(k+G)\cdot r}$, will include short wavelength $G \neq 0$ components which average to zero over the unit cell, so that $\bar{\phi}_{\rm tot} = \phi_{{\rm tot},G=0}(k)e^{ik\cdot r}$, and the right side of (22) becomes $\phi_0/\phi_{{\rm tot},G=0}(k) = \left(\epsilon^{-1}_{0,0}(k)\right)^{-1}$, where the last term is the inverse of the $(G,G') = (0,0)$ matrix element of the inverse microscopic dielectric response operator.

We thus conclude that, in the macroscopic limit,

$$\hat{k}^\dagger\bar{\epsilon}\hat{k} = \left(\lim_{|k|\to 0}\epsilon^{-1}_{0,0}(k)\right)^{-1}. \tag{22}$$

To evaluate (22), note that (21) gives

$$\epsilon^{-1}_{0,0}(k) = 1 + \frac{1}{\Omega}\frac{4\pi}{k^2}\hat{V}_0(k)X_{\rm ext}(k)\hat{V}_0^\dagger(k). \tag{23}$$

With the Fourier transform convention defined above, the asymptotic behavior of the components of the row vectors $\hat{V}_0(k)$ is

$$\hat{V}_0(k) \xrightarrow{k\to 0} -ik^\dagger P + \mathcal{O}(k^2), \tag{24}$$

where

$$P_{\alpha,n} \equiv \int d^3r\, V_n(r) r_\alpha \tag{25}$$

is a matrix of eigenfunction dipole moments. The limit of (23) is thus

$$\epsilon^{-1}_{0,0}(k) \xrightarrow{k\to 0} 1 + \frac{4\pi}{\Omega}\hat{k}^\dagger P X_{\rm ext}(k) P^\dagger\hat{k} + \mathcal{O}(k). \tag{26}$$

The external susceptibility matrix elements $X_{\rm ext}(k)$ themselves also exhibit anomalous k-direction behavior, due to the presence in (20) of $\bar{K}(k)$, which exhibits irregular $k \to 0$ behavior due to the singular nature of the $G = 0$ component of the diagonal operator $\hat{K}(k) = 4\pi/|k+G|^2$. Separating out the singular $G = 0$ term gives

$$\bar{K}(k) \xrightarrow{k\to 0} \bar{K}_H + \frac{4\pi}{\Omega}P^\dagger\hat{k}\hat{k}^\dagger P, \tag{27}$$

where $\bar{K}_H \equiv [\hat{V}(0)^\dagger K(k=0)\hat{V}(0)]_{G\neq 0}$ is the $k = 0$ Coulomb sum for electrostatic interactions among the columns of $\hat{V}$ but with the $G = 0$ omitted, what typical plane-wave implementations compute as the 'Hartree' interaction. Combining (20,27), then gives the small k behavior of $X_{\rm ext}(k)$ through a two-step renormalization process

$$\begin{aligned}\bar{X}_{\rm ext} &\xrightarrow{k\to 0} X_{\rm tot}(k=0)\left(1 - \bar{K}_H X_{\rm tot}(k=0)\right)^{-1}\\ X_{\rm ext}(k) &\xrightarrow{k\to 0} \bar{X}_{\rm ext}\left(1 - \frac{4\pi}{\Omega}P^\dagger\hat{k}\hat{k}^\dagger P\bar{X}_{\rm ext}\right)^{-1},\end{aligned} \tag{28}$$

as may be verified by direct substitution.

Finally, substituting (28) into (26) yields an expression whose inverse gives $\left(\epsilon^{-1}_{0,0}(k)\right)^{-1} = 1 - \frac{4\pi}{\Omega}\hat{k}^\dagger P\bar{X}_{\rm ext}P^\dagger\hat{k} + \mathcal{O}(k)$, as may be verified directly by multiplication to yield the identity. Substituting this last result in (22) and using the fact that $\hat{k}^\dagger\hat{k} = 1$ shows that the $k \to 0$ limit has precisely the correct tensor character, and gives the final result for the macroscopic dielectric tensor,

$$\bar{\epsilon} = 1 - \frac{4\pi}{\Omega}P\bar{X}_{\rm ext}P^\dagger, \tag{29}$$

with $\bar{X}_{\rm ext}$ defined explicitly as the $k \to 0$ limit in (28).

III. RESULTS

We apply the approximations of the previous section to the dielectric response of cubic ice and solid benzene. Ice and the benzene solid display two distinctly different types of intermolecular interactions: while ice contains strong hydrogen bonds, benzene only weakly interacts through van der Waals forces. A comparison of the two solids will provide insight into the limits and capabilities of our method.

We first calculate the macroscopic dielectric constant from the dielectric additive approximation to explore the convergence of the method as a function of included bands and eigenvectors. We investigate the accuracy and the assumptions of the dielectric additive approximations. We then present dielectric band structures for the separate additive approximations, and compare to the molecular and crystalline dielectric band structures.

A. Computational Details

The density-functional theory calculations and the subsequent dielectric calculations were performed in the open source, plane wave density functional theory software, JDFTx.[19] All calculations utilize the Perdew-Burke-Ernzerhof[20] (PBE) generalized gradient approximation (GGA) to the exchange-correlation functional, norm-conserving pseudopotentials generated in OPIUM[21] with the same functional, and a kinetic energy cutoff of 30 E_h (Hartree) for the plane-wave basis. The molecular calculations use a truncated Coulomb interaction to eliminate unwanted interactions between images in the supercell calculations.[22] Figure 1 schematically summarizes the method developed in section II to calculate the crystal dielectric response from the molecular response.

For the ice structure, we have chosen the simplest isomorph that obeys hydrogen bonding rules, the proton-ordered cubic ice XIc which has been theoretically proposed to be the true ground state of ice.[23] Neglecting a small tetragonal distortion, this structure consists of a two-molecule unit cell with the oxygen atoms on a diamond-cubic lattice with optimized cubic lattice constant 11.76 a_0 (Bohr). We perform the isolated single water molecule calculation for the additive approximation in a $3 \times 3 \times 3$ supercell.

For the benzene crystal, we use the experimentally-determined lattice parameters and carbon positions for the four-molecule orthorhombic unit cell,[24] and fill in the hydrogen positions by optimizing the density-functional geometry. We perform the isolated benzene molecule calculation in the crystal unit cell itself as it is sufficiently large.

We find that 500 bands are sufficient to converge the direct response calculation of both crystals, while 600 bands are sufficient for the isolated benzene molecule and 1000 bands are sufficient for the isolated water molecule (need more bands due to the larger supercell). We generate up to 50 eigenvectors per valence electron (which amounts to 400 eigenvectors for the water molecule and 1500 eigenvectors for the benzene molecule) to test the convergence of the dielectric response with eigenvectors; much fewer eigenvectors are actually necessary as we show below.

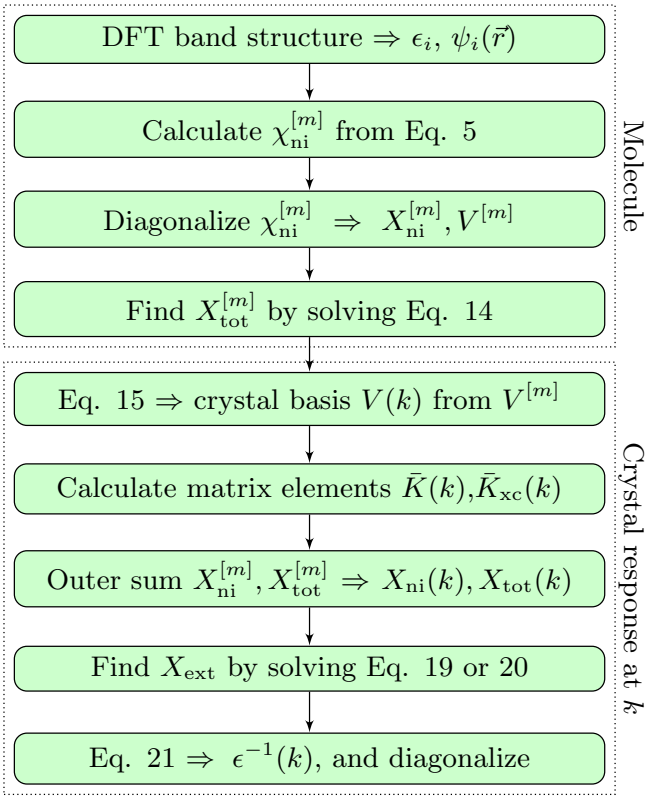

FIG. 1. Procedure to construct the crystal response from the molecular response using either the χ_{ni} or the χ_{tot} additivity approximations.

B. Bulk dielectric constants

The primary goal of the additive approximations developed here is to calculate the microscopic dielectric response. However, to explore the convergence of our calculations, we first calculate and compare the bulk dielectric constants, which can be computed directly as well as within approximate schemes such as our additive methods. Figure 2 shows the bulk dielectric constant computed directly for the crystals, from the molecular polarizability using the Clausius-Mossotti equation, and from the additive approximations for $\chi_{\rm tot}$ (11) and $\chi_{\rm ni}$ (10).

The first panel of Figure 2 depicts the convergence of the bulk dielectric function computed in the conduction-valence basis with the number of conduction-valence orbital pairs per electron. The second panel depicts the corresponding convergence for the $\chi_{\rm ni}$ eigenvector basis

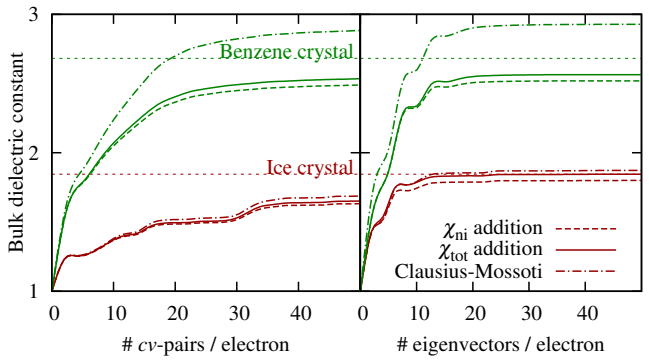

FIG. 2. Convergence of the average bulk dielectric constant (29) using the additive approximations for $\chi_{\rm tot}$ (11) and $\chi_{\rm ni}$ (10), as well as the Clausius-Mossotti equation, with respect to number of eigenvectors per electron (left panel) and number of conduction-valence pairs per electron (right panel). Dotted lines indicate the direct results for the crystals. Red lines indicate results for water and green for benzene.

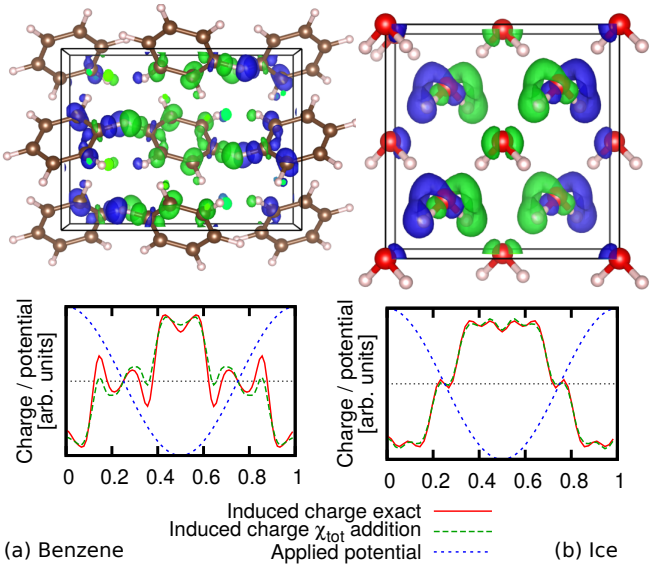

FIG. 3. Induced charge density in the (a) benzene and (b) ice crystals for a plane-wave applied potential with wavelength equal to (orthorhombic) unit cell length, calculated from the exact $\chi_{\rm ext}$ of the crystal, as well as from the the additive approximation (11). Top panels visualize the induced charge density (+ green, - blue) in the exact crystal calculation, while the lower panels compare the planarly averaged induced charge densities from the $\chi_{\rm tot}$-additive approximation with those from the exact crystal calculations.

with number of eigenvectors per electron. The eigenvector basis is clearly far more efficient and adequately converges the dielectric constant for water and benzene with 10 – 20 eigenvectors per electron. In contrast, more than 50 conduction-valence pairs per electron would be required to obtain comparable accuracy. The superiority of the eigenvector basis has been previously demonstrated for the direct calculation of the dielectric response of molecules or crystals,[15–17] while Figure 2 shows that this superior efficiency also extends to the reconstruction of the crystal response from the molecular one using our method.

Now we focus on the converged dielectric constants in the second panel of Figure 2. The Clausius-Mossotti equation and the two additive approximations agree very well with the direct crystal calculation for the dielectric constant of ice (red lines). The best agreement is obtained with the $\chi_{\rm tot}$ additivity approximation, and the Clausius-Mossotti equation overestimates the dielectric constant. In comparison, for the benzene crystal dielectric constant (green lines), the approximate dielectric constants agree less well with that of the direct calculation. The Clausius-Mossotti equation approximates the reaction field of surrounding molecules as a spherical cavity which results in an overestimation for the planar benzene molecule (which is less spherical than the water molecule). The $\chi_{\rm ni}$ and $\chi_{\rm tot}$ additivity approximations fully account for the geometry of the molecule and agree better with the direct calculation, but they systematically underestimate the bulk dielectric constant. Regardless, the $\chi_{\rm tot}$ additivity approximation yields the best agreement in both systems.

We expect that the additive approximations are less accurate for the benzene crystal than for ice because the additive approximation localizes charge to each molecule, yet the benzene crystal has significant orbital overlap between neighbours. To further explore this possible limitation of our theory, Figure 3 compares the induced charge densities of the crystals in response to a low wave-vector plane-wave applied potential, as calculated directly and from the additive approximations. The induced charge densities agree well for the ice crystal, but exhibit discrepancies in the interstitial region between molecules for the benzene crystal because the additive approximation does not account for the effects of overlap between molecules.

We further confirm the effect of intermolecular orbital overlap by investigating the variation of the accuracy of the additive approximations for the dielectric constant with crystal strain. The intermolecular overlap decreases exponentially with separation, so we expect its contribution to reduce dramatically at moderate strains. Indeed, Fig. 4 shows that the accuracy of the additive approximations for ice remains excellent, while that for benzene improves substantially, as expected. The Clausius-Mossotti approximation for the benzene crystal still exhibits larger errors because it is dominated by the non-spherical nature of the molecule, unrelated to the overlap. We expect that the additive approximations will be more accurate for higher band-gap molecular semiconductors and insulators (eg. ice) due to the induced charge localization. Extensions of the approximation that better treat delocalization, perhaps accounting for intermolecular kinetic energy matrix elements, could better describe lower-band gap molecular semiconductors such as benzene.

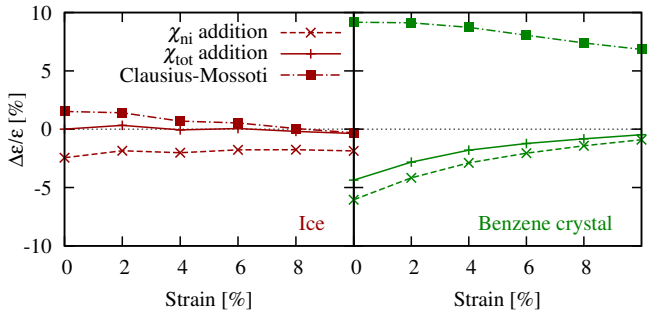

FIG. 4. Comparison of percentage errors in bulk dielectric constant approximations for ice and the benzene crystal as a function of strain. The error is calculated with respect to the direct (strained) crystal calculations.

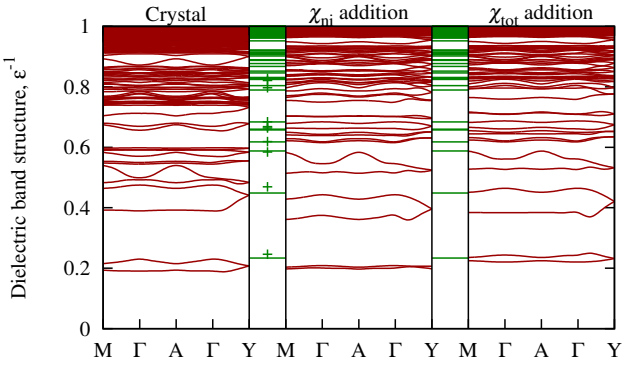

FIG. 5. Ice dielectric band structure of the crystal compared to the additive approximations for χ_{ni} (10) and χ_{tot} (11). Molecular levels of water in vacuum (green lines) and implicitly solvated[25] water (green +) are shown between the crystal and additive approximation band structures for reference.

C. Dielectric band structure

The microscopic dielectric response, conveniently represented using the dielectric band structure, is important for calculating RPA correlation energies. Unlike the bulk dielectric constant, the calculation of the microscopic response for large unit cells is memory intensive and computationally expensive. In our approach, the computational limits apply to the molecular response rather than the extended structure. Here, we benchmark the approach in crystals with small to moderate unit cells where we can perform the direct calculation to provide a comparison, but the real power of our method is that it extends trivially to disordered structures and snapshots of liquids where the direct calculation would be prohibitively expensive.

To develop intuition about dielectric band structures, we compare the directly calculated dielectric bands for an ice crystal with the dielectric levels for an isolated water molecule in the first two panels of Figure 5. The molecular and crystal levels are similar, except that the molecule does not have the k-point dependent band structure of the crystal. The molecular dielectric levels are split by the exchange-correlation and Coulomb interactions between the molecules, leading to the crystalline dielectric band structure in Figure 5. For instance, the lowest molecular dielectric level splits into two bands in the crystalline calculation which correspond to parallel and antiparallel polarizations of the two water molecules in the unit cell (in analogy with molecular orbital theory for the electronic states).

Additionally, to investigate if the response of the molecule is affected by the potential due to the neighbors, Figure 5 displays the dielectric levels for a solvated water molecule calculated using a solvation model that accurately captures the solvation energy and dipole moment of a water molecule in liquid water.[25] The solvated water molecule's dielectric band structure, which in turn we expect to closely resemble that of one molecule in the crystal potential, is very similar to that of the molecule in vacuum. This indicates that while the environment of the crystal is different than that of the vacuum, it perturbs the molecule linearly so that the response functions of each molecule do not change appreciably from isolation to in the liquid or solid environment. Note that the solvated dielectric bands that remain unchanged correspond to the response of a single molecule in the liquid environment to fields *external to that molecule*; the net response to fields external to the liquid or solid does indeed differ from the isolated molecule (and corresponds precisely to the crystal dielectric band structure for the solid).

Next, we examine the two additive approximations χ_{tot} (11) and χ_{ni} (10), and determine which approach is more accurate and hence suitable for future RPA calculations of large / disordered systems. Both additive approximations produce dielectric band structures which closely approximate that of the ice crystal, as shown in the center and last panels of Figure 5, but χ_{tot} addition yields better agreement while χ_{ni} addition slightly underestimates the band splitting, due to an underestimation of the interactions between polarizations of the molecules in the crystal. Both approximations slightly underestimate the dispersion in the bands of the direct crystalline calculation. This could potentially be corrected in future work by additionally accounting for intermolecular kinetic energy interactions, estimated using a Thomas-Fermi local density approximation[26,27] (optionally with gradient corrections).

Figure 6 shows the corresponding results for the benzene crystal. With four molecules per unit cell, the splittings are more complicated and difficult to identify intuitively. However, the remarkable agreement between the additive approximations and the much more expensive direct crystalline calculations remains evident. Just as in the ice calculation, the χ_{ni} additivity approximation (10) slightly underestimates the band splitting, and both approximations slightly underestimate the dispersion compared to the bands in the direct crystalline calculation. Additionally, the overestimation of the first eigenvalue

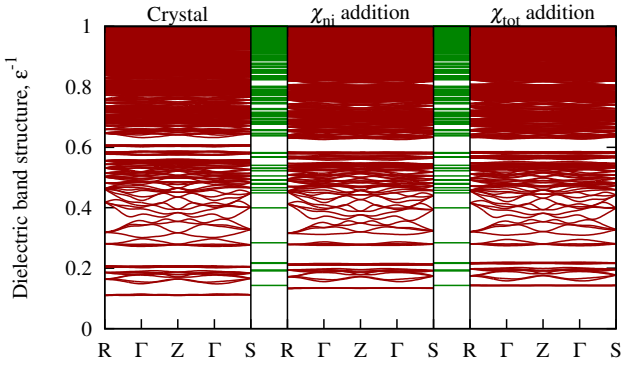

FIG. 6. Analogous to Figure 5 for the benzene crystal.

in the additive approximations is due to the assumption that the charge is localized to the molecule, as discussed previously in the context of the underestimated bulk dielectric response.

The agreement of approximate dielectric band structures with the direct calculations is promising for applications such as RPA correlation energies of large configurations of molecules. Ultimately, the adequacy of this approximation for such applications will be tested by linking our framework for approximate dielectric functions with an RPA code and explicitly comparing the calculated correlation energies.

IV. CONCLUSIONS

This work develops a theoretical approach to determine the full microscopic dielectric response of a molecular crystal from the microscopic response of its constituent molecules. We argue that it is possible to approximately decompose the non-interacting (Kohn-Sham) as well as total-field susceptibilities as a sum of molecular contributions. In particular, we find that eigenvectors of the molecular response function form an excellent (yet non-orthogonal) basis for the response of the crystal.

We then test the feasibility of this approach by comparing the dielectric band structures calculated from the molecular decomposition with much more expensive direct crystalline calculations. We find remarkable agreement in the predicted response of ice, and very good agreement for that of benzene. Our additive approach does not capture the intermolecular charge delocalization contribution to the benzene dielectric constant, leading to its underestimation. However, our method is still generally applicable to molecular materials that do not display large amounts of orbital overlap. We expect that our method will perform well for molecular systems that are electronically insulating, but semiconducting materials such as the benzene crystal will require an extension to our approach to capture this additional contribution to the dielectric response. Future work will address this potential extension, possibly by including the effects of a kinetic energy functional.

We also derive a formalism for computing the macroscopic dielectric tensor of a molecular crystal, which is much cleaner than the general theory for arbitrary crystals due to the localization of the induced dipole moments. On the other hand, this formalism retains full microscopic detail and does not reduce the molecules to point dipoles or multipoles as in the Clausius-Mossotti relation or its generalizations.

For simplicity and clarity, this work focused on the dielectric response predicted using density functional theory. However it also outlines the calculation of crystal responses using quantum chemical methods that describe higher-order correlation effects. In essence, this would involve generating a good basis using the density-functional response eigenvectors of the molecule, performing a series of perturbation calculations using the quantum chemical method on a single molecule, and then putting together the crystalline response using the additive approximation formalism established in this work. It would be extremely interesting to apply this method to study the dielectric response of systems in which the molecular response are strongly affected by correlation effects.

Finally, the additive approximation and the molecular decomposition formalism presented here can be applied more generally, rather than just to crystalline systems, which we chose for ease of initial computational implementation and for the feasibility of the direct calculation to benchmark our approximations. The real power of our method lies in its potential application to non-periodic systems, where direct calculations are impractical. In particular, this would enable calculating the microscopic dielectric properties of molecular nanostructures, fully accounting for the effects of surfaces and defects. This would also enable the rapid calculation of the dielectric response of multiple snapshots of molecular fluids from a single molecule response calculation, leading eventually towards correlated *ab initio* molecular dynamics calculations.

ACKNOWLEDGEMENTS

This work was supported as a part of the Energy Materials Center at Cornell (EMC^2), an Energy Frontier Research Center funded by the U.S. Department of Energy, Office of Science, Office of Basic Energy Sciences under Award Number DE-SC0001086.

K.A.S was financially supported by a National Science Foundation Graduate Research Fellowship.

[1] S. Forrest. *Nature*, 428:911–918, 2004.
[2] S.Guo, S. Kim, S. Mohapatra, Y. Qi, et al. *Advanced Materials*, 24:699–703, 2011.
[3] I. McCulloch, M. Heeney, C. Bailey, et al. *Nature Materials*, 5:328 – 333, 2006.
[4] J. Luria, K. Schwarz, M. Jaquith, R. Hennig, and J. Marohn. *Advanced Materials*, 23:624–628, 2010.

[5]H. Heitzer, T. Marks, and M. Ratner. *JACS*, 136:9753–9759, 2013.
[6]H. Nguyen and G. Galli. *J. Chem. Phys.*, 132:044109, 2010.
[7]D. Lu, Y. Li, D. Rocca, and G. Galli. *Phys. Rev. Lett.*, 102:206411, 2009.
[8]H. Nguyen and S. de Gironcoli. *Phys. Rev. B*, 79:205114, 2009.
[9]A. Baldereschi and E. Tosatti. *Solid State Comm.*, 29:131, 1979.
[10]M.S. Hybertsen and S.G. Louie. *Physical Review B*, 35:5585–5601, 1987.
[11]W. Kohn and L. Sham. *Phys. Rev.*, 140:A1133, 1965.
[12]F. Bruneval and X. Gonze. *Phys. Rev. B*, 78:085125, 2008.
[13]P. Umari, G. Stenuit, and S. Baroni. *Phys. Rev. B*, 81:115104, 2010.
[14]L. Reining, G. Onida, and R.W. Godby. *Phys. Rev. B*, 56, 1997.
[15]D. Lu, F. Gygi, and G. Galli. *Physical Review Letters*, 100:147601, 2008.
[16]H. Wilson, F. Gygi, and G. Galli. *Physical Review B*, 78:113303, 2008.
[17]H. Wilson, D. Lu, F. Gygi, and G. Galli. *Physical Review B*, 79:245106, 2009.
[18]For crystals with primitive cells containing multiple molecules, we formally consider the primitive cell as a 'meta-molecule', with the states of each separate molecule represented as a block of columns in $V^{[m]}$ and the corresponding matrix elements appearing in diagonal blocks in $X^{[m]}_{\text{ext}}$ and $X^{[m]}_{\text{tot}}$.
[19]R. Sundararaman, D. Gunceler, K. Letchworth-Weaver, K. A. Schwarz, and T. A. Arias. JDFTx. `http://jdftx.sourceforge.net`, 2012.
[20]J. P. Perdew, K. Burke, and M. Ernzerhof. *Phys. Rev. Lett.*, 77:3865, 1996.
[21]OPIUM. *Pseudopotential generation project*. `http://opium.sf.net`.
[22]R. Sundararaman and T.A. Arias. *Phys. Rev. B*, 87:165122, 2013.
[23]Z. Raza, D. Alfe, C. G. Salzmann, J. Klimes, A. Michaelides, and B. Slater. *Phys. Chem. Chem. Phys.*, 13:19788–197595, 2011.
[24]E.G. Cox, F.R.S, D.W.J. Cruickshank, and J.A.S. Smith. *Proc. R. Soc. Lond. A*, 247, 1958.
[25]R. Sundararaman and W.A. Goddard. *J. Chem. Phys.*, 142:064107, 2015.
[26]L. H. Thomas. *Proc. Cambridge Phil. Soc.*, 23:542, 1927.
[27]E. Fermi. *Rend. Accad. Naz. Lincei*, 6:602, 1927.

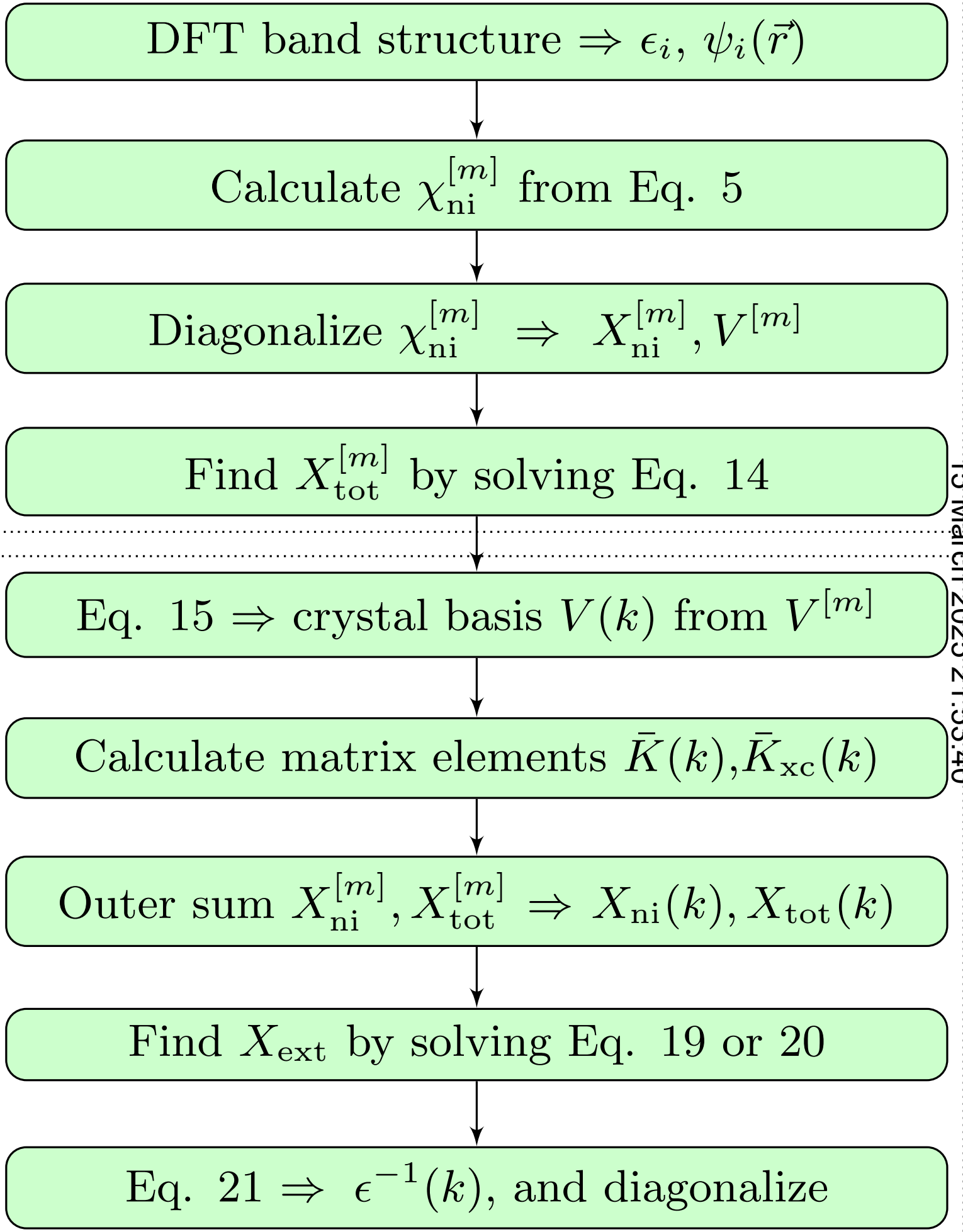

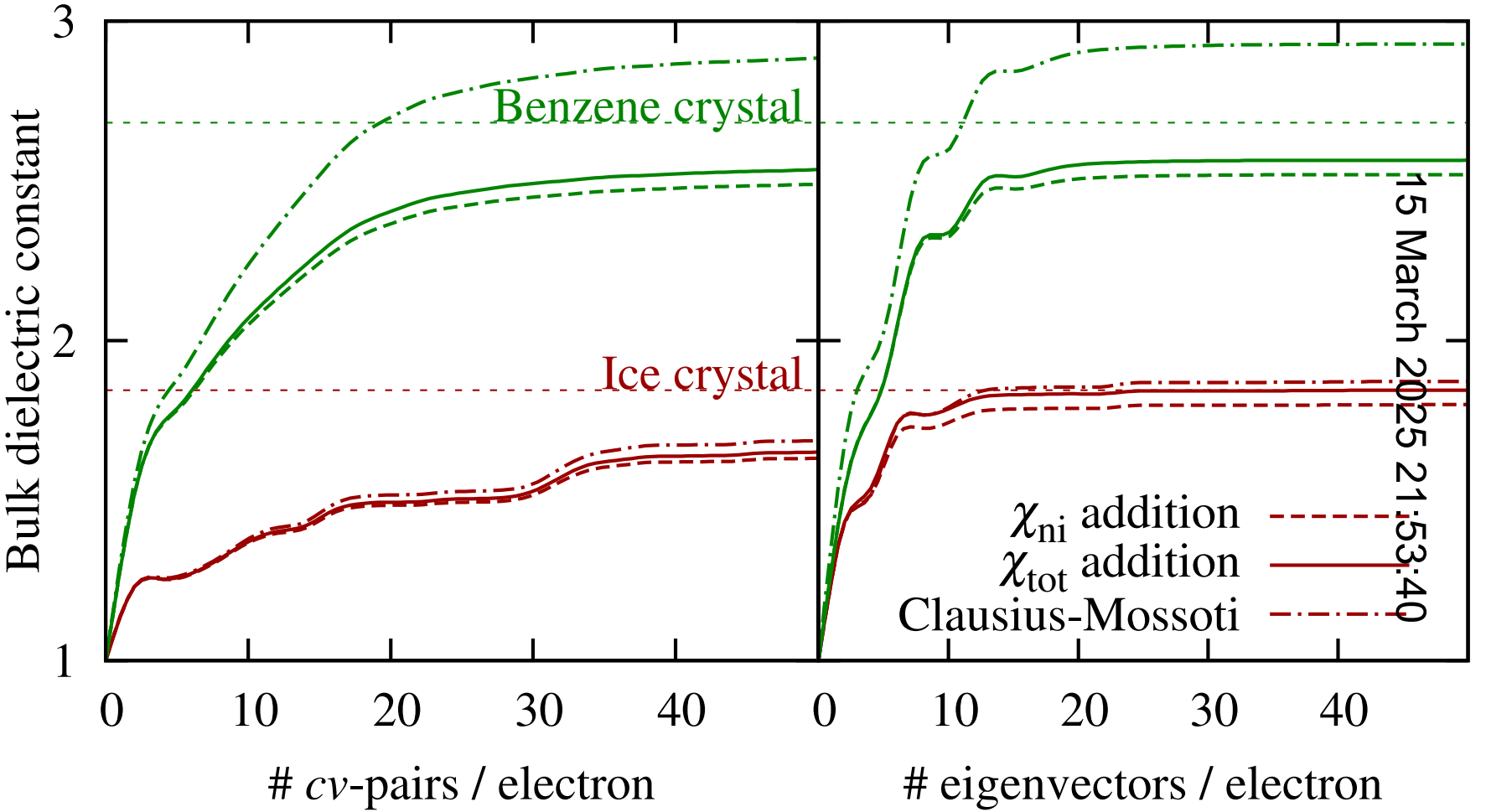
Bulk dielectric constant
3
2
1
Benzene crystal
Ice crystal
0
10
20
30
40
cv-pairs / electron
eigenvectors / electron
χni addition
χtot addition
Clausius-Mossoti
15 March 2025 21:53:40

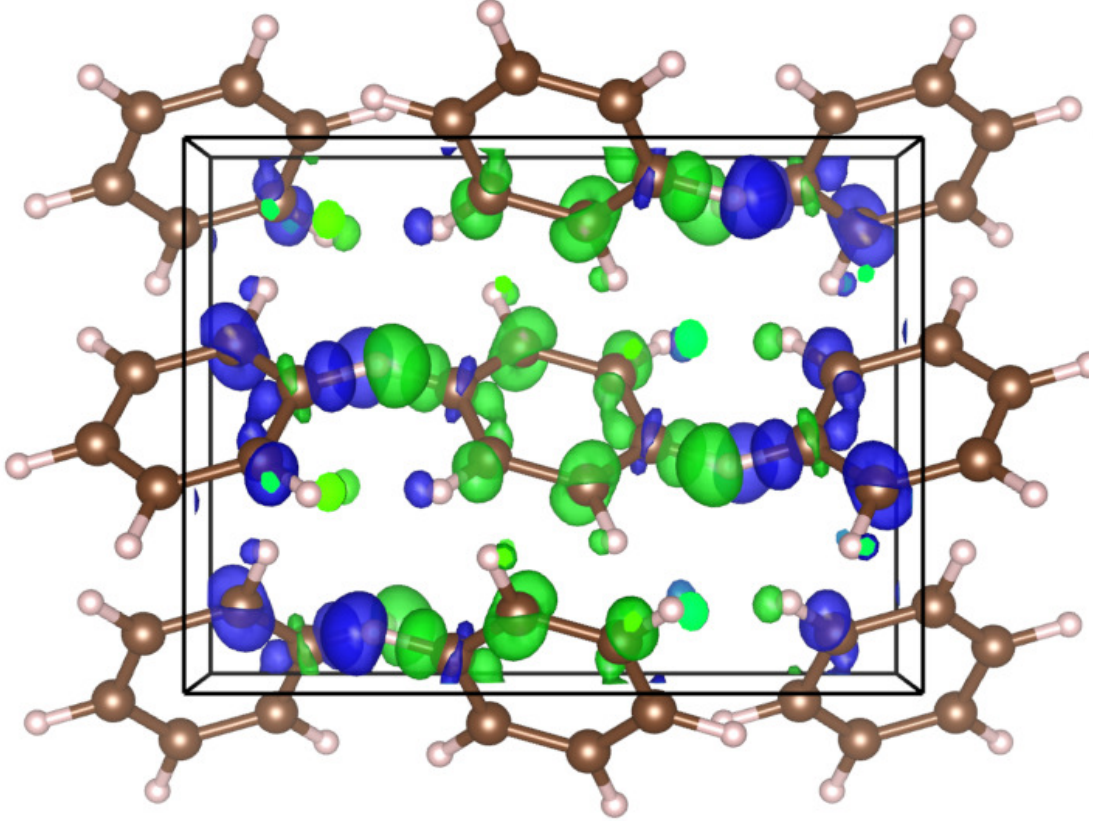

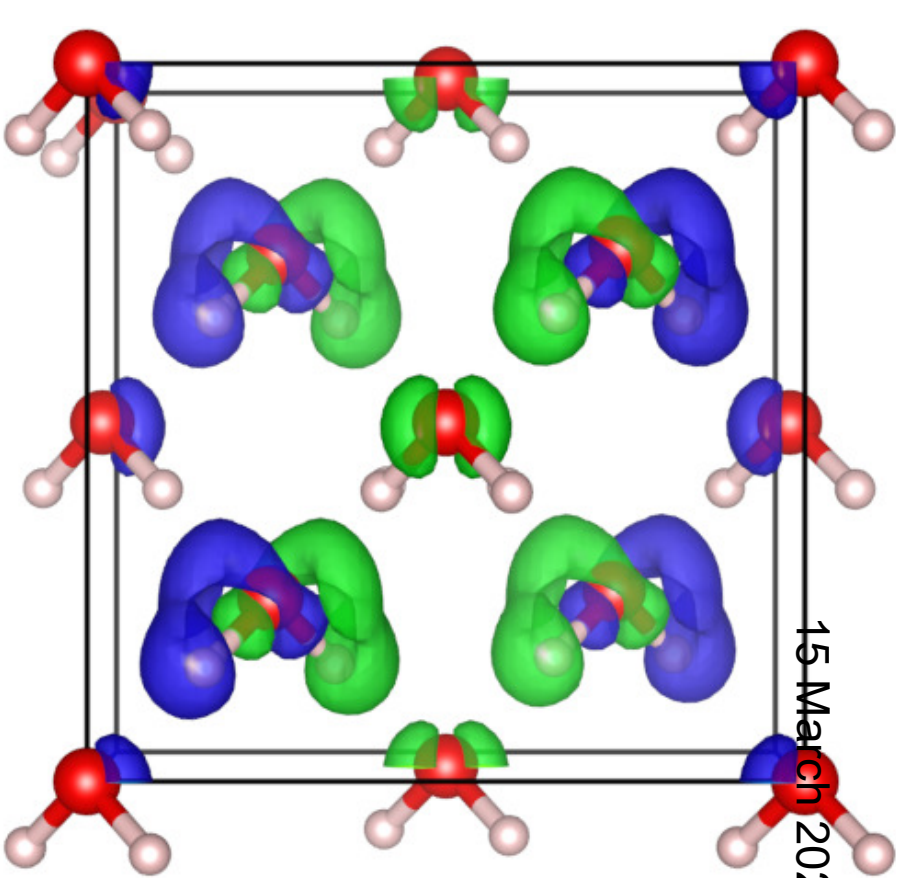

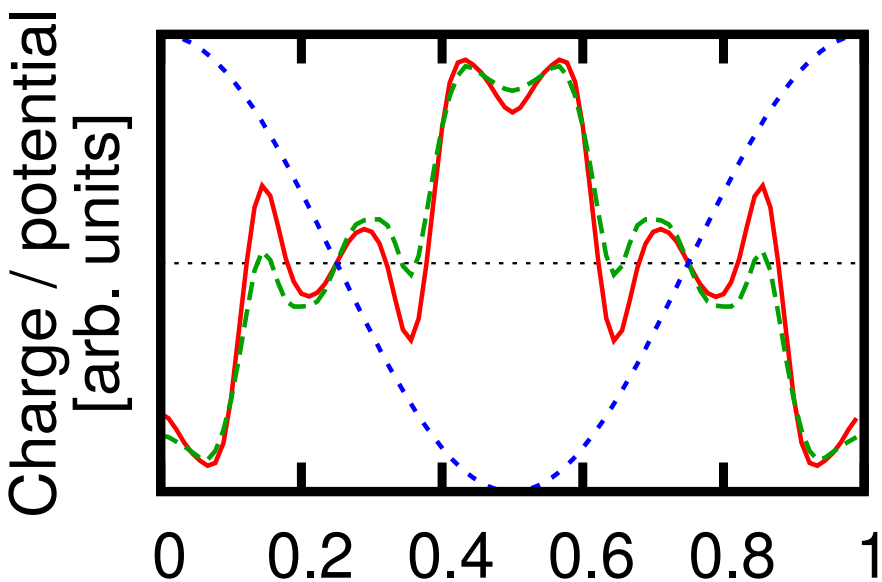

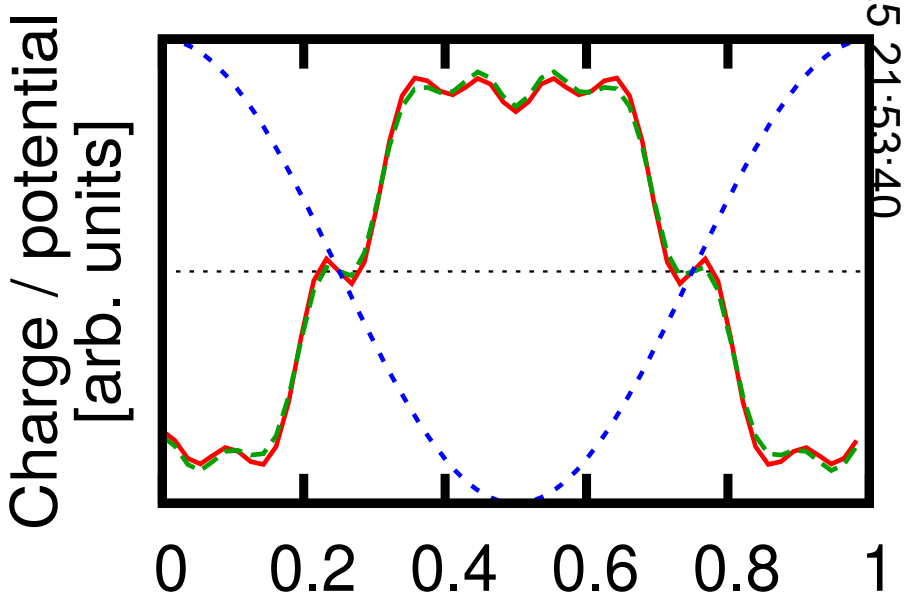

Induced charge exact

Induced charge χ_{tot} addition

Applied potential

(a) Benzene

(b) Ice

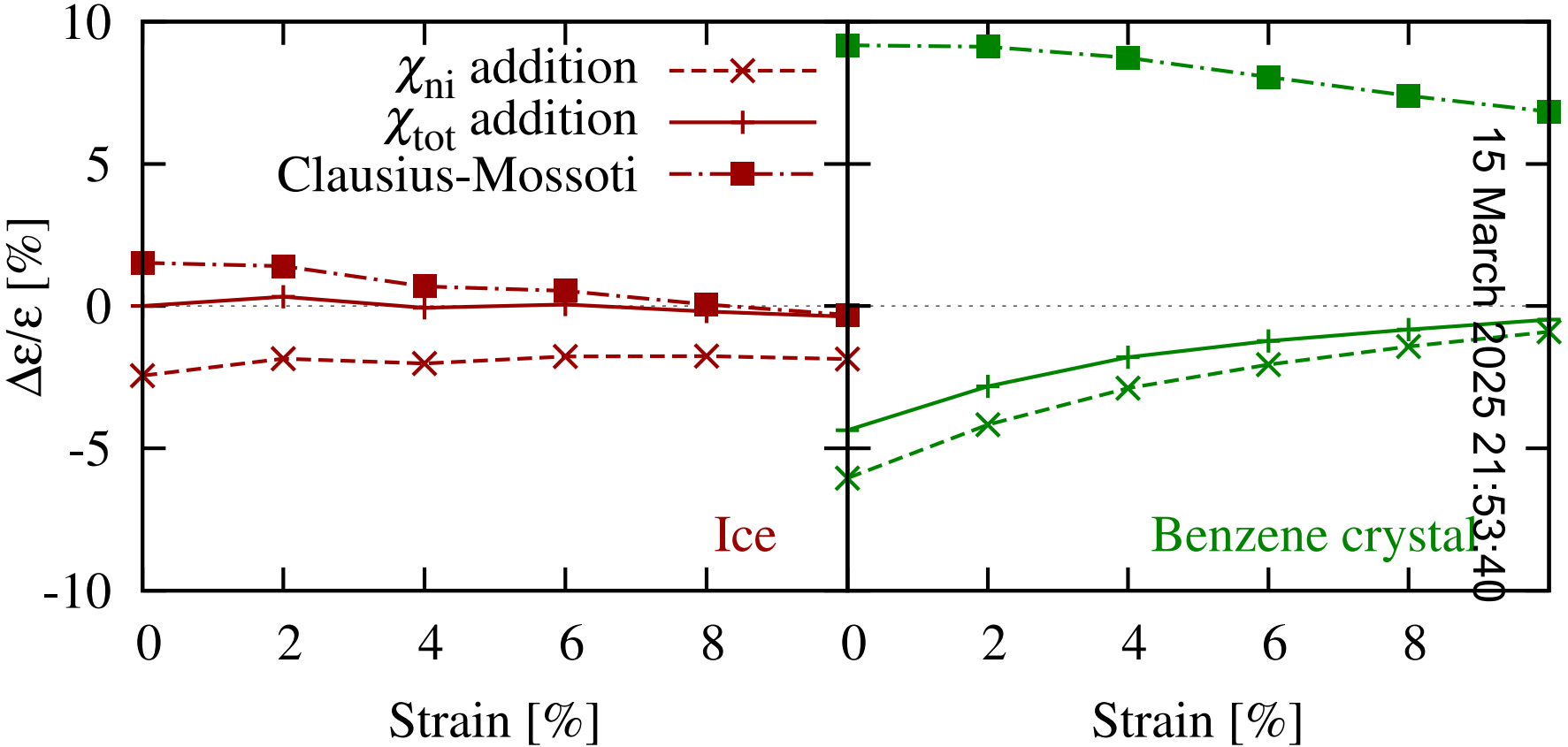
10
5
0
-5
-10
Δε/ε [%]
χni addition
χtot addition
Clausius-Mossoti
Ice
Benzene crystal
0
2
4
6
8
Strain [%]
Strain [%]
15 March 2025 21:53:40

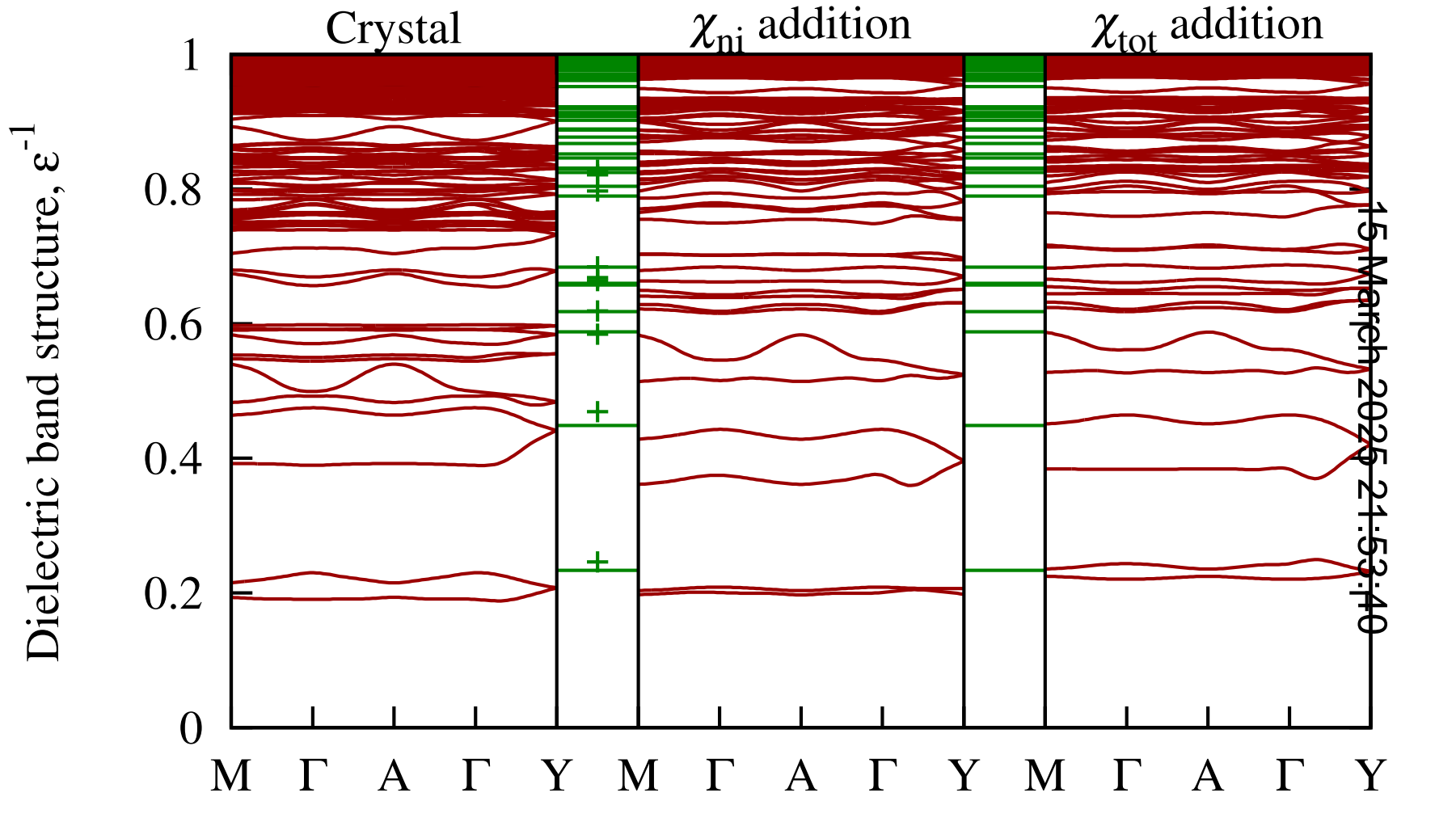
Crystal
χ_{ni} addition
χ_{tot} addition
Dielectric band structure, ε^{-1}
1
0.8
0.6
0.4
0.2
0
M Γ A Γ Y M Γ A Γ Y M Γ A Γ Y
15 March 2025 21:53:40

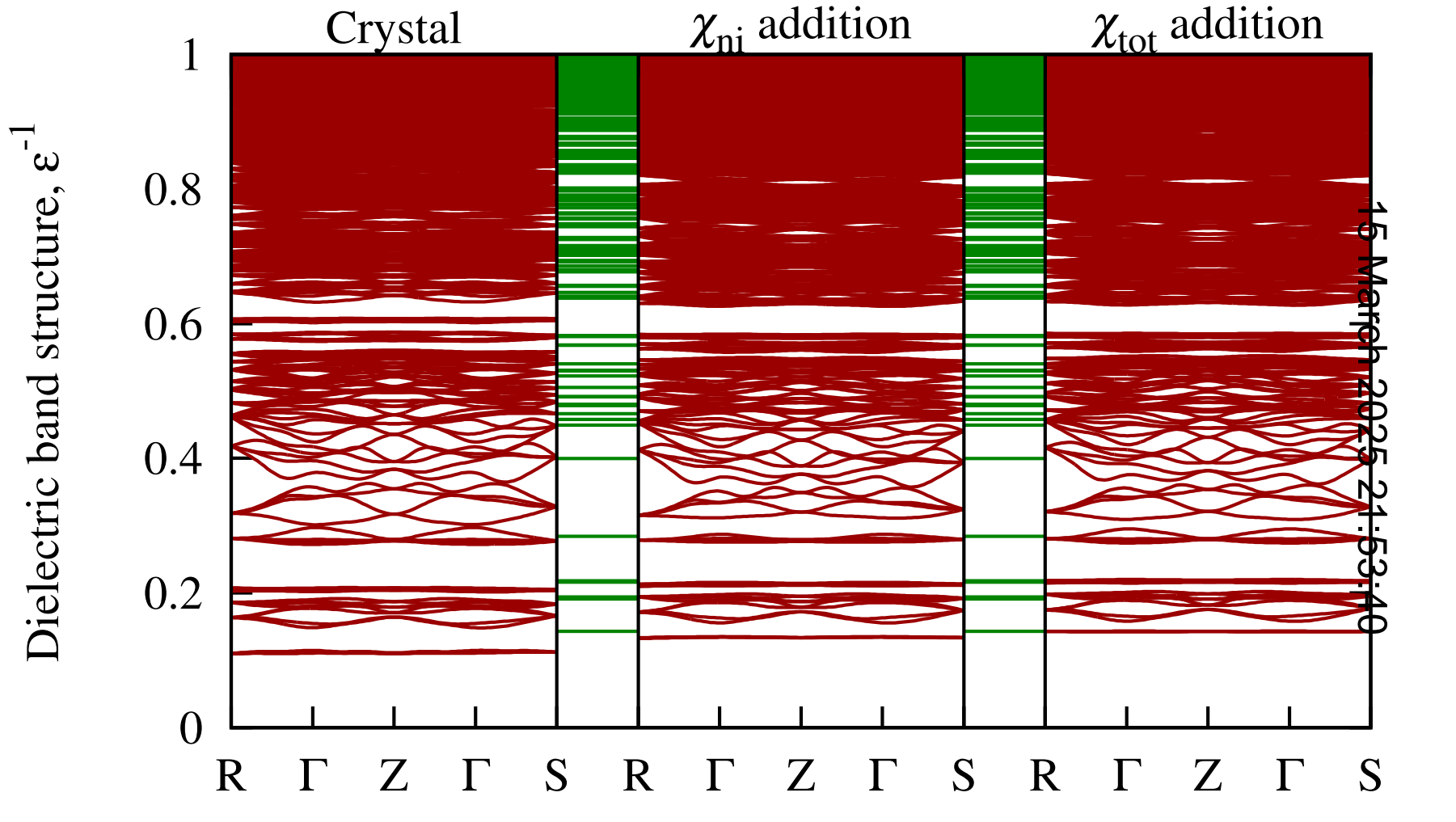
Crystal
χ_{ni} addition
χ_{tot} addition
Dielectric band structure, ε^{-1}
1
0.8
0.6
0.4
0.2
0
R Γ Z Γ S R Γ Z Γ S R Γ Z Γ S
15 March 2025 21:53:40